Measurement of the speed of X-rays

E. Zolotoyabko[a]* and J. P. Quintana[b]

[a]Department of Materials Engineering, Technion – Israel Institute of Technology, Haifa 32000, Israel, and [b]DND-CAT Research Center, Northwestern University, APS/ANL Sector 5, Building 432A, 9700 South Cass Avenue, Argonne, IL 60439-4857, USA. E-mail: zloto@tx.technion.ac.il

X-ray pulses from the Advanced Photon Source at Argonne National Laboratory were used to measure the speed of X-rays in the energy range between 21 and 60 keV. An $LiNbO_3$-based 0.58 GHz surface acoustic wave device served as a temporal analyzer in the stroboscopic time-resolved diffraction measurements. By synchronizing the surface acoustic wave excitation and periodic X-ray illumination of the $LiNbO_3$ crystal, the temporal modifications in the $LiNbO_3$ diffraction profiles could be followed and the time points of X-ray arrivals at the analyzer position for different analyzer to storage ring distances determined. The speed of the X-rays was determined as the ratio of measured spacings and corresponding delay time intervals. Within the experimental error bars, the obtained X-ray velocities converged to the tabulated constant for the speed of light in a vacuum.

Keywords: speed of light; X-ray diffraction; fast time-resolved measurements.

1. Introduction

After 1983, the speed of light is published in handbooks as an exact constant (Cohen & Taylor, 1987). Consequently, with no uncertainty in the value, some other physical constants can be precisely defined in terms of the speed of light. More than 300 years of scientific efforts and developments since Roemer's first astronomic observations on Jupiter's satellites preceded the current situation. Comprehensive reviews of the history of light speed measurements can be found by Bergstrand (1956), Sanders (1965) and Froome & Essen (1969). When the number of independent measurements became large, statistical methods of data treatment were applied. Results obtained by different methods [mainly by microwave interferometry and by the visible-light time-of-flight (geodimeter) method (Bergstrand, 1956; Froome & Essen, 1969)] were found to be converging to the same value within better than a p.p.m. precision (Taylor *et al.*, 1969). At the end of the 1970s, a 10^{-9} level of accuracy had been achieved by using lasers and phase-locked oscillators (Bates, 1988).

All of these measurements were accomplished with photon wavelengths $\lambda > 0.5$ μm. Up to now, direct laboratory experiments with high-energy photons have not been performed. For higher-energy photons, such measurements are much more complicated due to significantly lower intensities and difficulties in manipulating with high-energy photon beams. However, the high brilliance of third-generation synchrotron sources offers us the principal possibility to perform time-of-flight experiments with X-rays, yet with less precision than with visible-light optics.

In this paper, we report on the first direct measurements of the velocity of electromagnetic waves in the X-ray range of wavelengths by utilizing synchrotron radiation from the Advanced Photon Source (APS) at Argonne National Laboratory. We used the stroboscopic principle of registration to detect in a time-resolved mode the X-rays diffracted from a piezoelectric $LiNbO_3$ crystal under high-frequency acoustic wave excitation. Third-generation synchrotron sources are very suitable for fast time-resolved experiments because the outgoing radiation has a well defined temporal pulsed structure, which allows us to avoid using a primary chopper. In fact, for an individual observer, the ultra-relativistic electrons, circulating inside the synchrotron storage ring, produce very short (∼50–100 ps) X-ray bursts only at those instants when electron bunches intersect the observer's line of view. A vibrating piezoelectric crystal serves as a temporal analyzer of X-ray arrivals from the storage ring to the experimental hutch, *i.e.* it acts, in some sense, as a Kerr cell in optical measurements (Sanders, 1965). Consequently, the speed of X-rays can be measured if their travelling distance to analyzer is changed.

2. Experimental technique

The key issue of our experiment is to synchronize the X-ray bursts with the time-dependent deformation induced within the piezoelectric crystal by a high-frequency standing acoustic wave. This deformation field, in turn, affects the spatial and temporal distributions of the diffracted X-rays (see, for example, Zolotoyabko *et al.*, 1993, 1998), depending on the phase, φ, between the deformation wave and periodic X-ray illumination. In general, the periodic high-frequency deformation within an almost perfect crystal causes angular satellites to appear in the diffraction profile (Entin & Assur, 1981). However, under standing-wave conditions, the deformation of the entire crystal lattice equals zero twice per period. Consequently, the diffraction profiles recorded with X-rays which arrive synchronously with these null points are the same as the pattern from an undisturbed crystal lattice. Therefore, the satellite intensity, measured as a function of φ, can be used for fast time-resolved measurements.

The phase, φ, between the periodic X-ray illumination and acoustic wave can be varied either by means of electronic delay lines or by changing the distance between the piezoelectric crystal and the storage ring. In the latter case, the points of zero-effect are separated by distance $\Delta L_0 = L_{j+1} - L_j = c_x/2\nu$, depending on the speed of X-rays, rays, c_x, and a well defined acoustic frequency, ν. From the experimental point of view, in order to measure c_x, the distance ΔL_0 should be as short as possible, impelling us to work with high-frequency surface acoustic waves (SAW). The SAW devices used in current experiment provide $\nu = 0.58$ GHz, which corresponds to $\Delta L_0 = 25.85$ cm.

SAW devices (see Fig. 1) were produced on the polished surfaces of *Y*-cut $LiNbO_3$ wafers, 76 mm in diameter and 0.5 mm thick. For device fabrication, 300 μm-wide strips of interdigital electrodes consisting of 1.5 μm metal fingers separated by 1.5 μm blank intervals were deposited using lift-off photolithography. The SAW wavelength, $\lambda_s = 6$ μm, is twice the distance between adjacent electrodes (Matthews, 1977). After deposition, the wafers were cut to rectangular specimens of area 10 × 20 mm. The transmission measurements of the energy losses in the SAW devices by means of an RF network analyzer (HP 8712 ET) revealed resonant spectra centred at 0.581 GHz (which is expected for *Z*-propagating SAW) and having a band width of 7 MHz (see Fig. 1).

Diffraction measurements were carried out at the 5BMD beam station which is located about 60 m away from the storage ring. X-rays travelled within an evacuated tube (vacuum 10^{-7} torr) to prevent X-ray absorption by air. Refraction corrections to the speed of X-rays are negligible, as compared with the visible light optics, because even in crystals the X-ray refraction index, $n = 1 - \xi$, is very close to 1 ($\xi \simeq 10^{-5}$). Diffraction measurements were performed using a four-circle Huber diffractometer, which was mounted on a Thomson motorized linear stage. The latter provided the diffract-

ometer translation along an incident beam in steps of 100 nm. The position of the piezoelectric crystal (SAW device) during the measurement period was monitored with a 100 nm precision by a laser-scan micrometer (Mitutoyo LSM-6000).

Diffraction profiles (rocking curves) were recorded in the reflecting Bragg scattering geometry from the (030) and (060) $LiNbO_3$ atomic planes parallel to the crystal surface. The diffraction geometry is also illustrated in Fig. 1. A primary beam was monochromated by using Si(333) reflections from the double-crystal monochromator. Measurements were performed at five different energies: 21, 30, 42, 51 and 60 keV. The beam from the double-crystal monochromator was restricted in spatial dimensions to 50 μm vertically and 200 μm horizontally using slits. Small beam size is absolutely necessary to observe pronounced angular satellites in diffraction profiles. The diffraction signal was taken from the SAW device area beneath the interdigital electrodes where the standing surface acoustic wave is formed (Matthews, 1977).

The principal scheme of the time-resolved diffraction measurements is shown in Fig. 2. The electron bunch pattern of the APS storage ring consisted of the main 22 singlets, separated by 153.44 ns, which provided X-ray bursts with a frequency of ν_r = 6.517 MHz. Besides that, there were six bunches separated by 2.841 ns and shifted by 460 ns relative to the group of 22 singlets. In our measurements, the sample excitation was synchronized with the periodicity of the 22 singlets.

For this purpose, electric pulses with frequency ν_r from a bunch clock generator were passed through a programmable delay unit and applied to the input of the signal synchronizer. The latter generated a phase-locked sinusoidal signal of multiple frequency, $\nu = N\nu_r$ ($N = 89$).

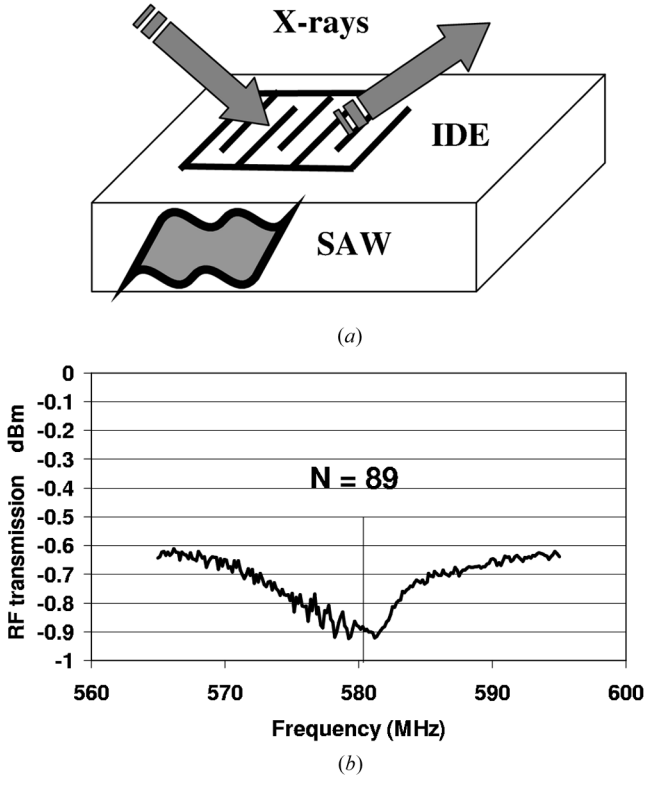

Figure 1
(*a*) X-ray beam incident onto an $LiNbO_3$-based SAW device. IDE stands for interdigital electrodes. (*b*) Frequency-dependent energy losses (transmission) in the SAW device. The vertical line shows the working frequency of $\nu = 89\nu_r$.

After amplification to approximately 7 V peak to peak, the signal was applied to the interdigital electrodes of the SAW device. Direct measurement of the SAW frequency in the phase-locked mode yielded ν = 580028700 ± 80 Hz. The phase locking affords a rigid phase relation between the acoustic and X-ray signals during a diffraction scan (see, for example, Zolotoyabko *et al.*, 1999), which takes a few minutes. By means of a programmable delay unit, this phase relation could be changed in a controlled way (the minimal temporal step was 18 ps), thus modifying an acoustic effect on X-ray diffraction. Alternatively, the time delay can be introduced by controlled translation of the diffractometer with the analyzing SAW device along the incident beam.

3. Results

With no ultrasound, the rocking curves (see Fig. 3*a*) measured with a highly restricted and quasi-parallel X-ray beam are very narrow (FWHM ≃ 1 arcsec), indicating high structural quality of the $LiNbO_3$ crystals. As was mentioned, an acoustic wave creates a periodic deformation field which modulates the electron density and gives rise to angular satellites in the rocking curve (Fig. 3*b*). Satellites (Stokes and anti-Stokes components) in the vicinity of the main diffraction maximum appear as a result of inelastic X-ray scattering with creation and annihilation of acoustic phonons of a given frequency and wavevector, *i.e.* as a result of the X-ray Brillouin scattering. Satellites of the *n*th order reflect a contribution from inelastic scattering with participation of *n* phonons. The phonon energy for a frequency of 0.58 GHz is only E = 2.4 μeV, which is three orders of magnitude lower than the registration limit of modern inelastic X-ray scattering techniques (Masociovecchio *et al.*, 1996). However, the momentum transfer can be easily detected by high-resolution X-ray diffraction. Based on the energy and momentum conservation laws, an angular distance, $\Delta\Theta_s$, between adjacent satellites is $\Delta\Theta_s = d/\lambda_s$, where d is the interplanar distance (d-spacing) for the X-ray reflection used and λ_s is the acoustic wavelength (see, for example, Zolotoyabko &

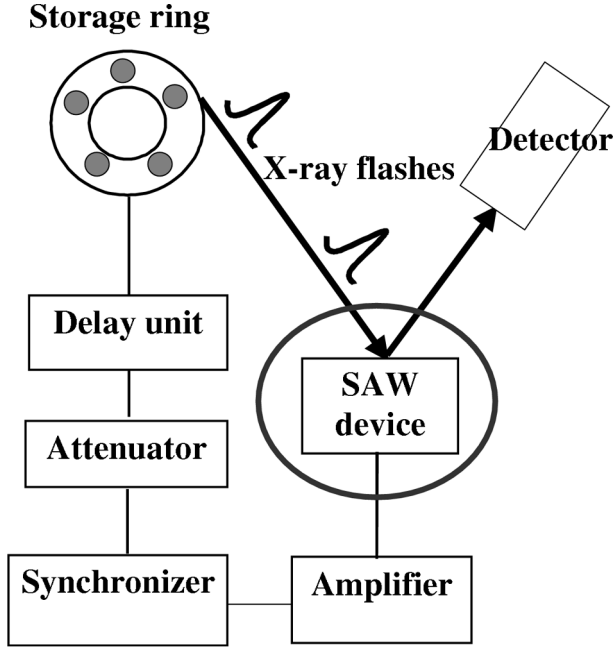

Figure 2
Schematic diagram of the time-resolved measurements.

Polikarpov, 1998). In our case, $\Delta\Theta_s$ = 2.56 arcsec, *i.e.* satellites are well separated from the main diffraction maximum. This is the first observation of diffraction satellites induced by a standing SAW. Recently, diffraction satellites induced by travelling SAW have been observed in GaAs at 579 MHz (Sauer *et al.*, 1999) and in Si at 365 MHz (Tucoulou *et al.*, 2000).

As is seen in Fig. 3(*b*), the satellite intensity can reach 40% of the main peak intensity, *i.e.* the SAW device acts as an effective and fast temporal modulator for X-rays. The satellite contribution to the diffraction intensity depends on the acoustic deformation within the crystal at a time point of X-ray illumination and, hence, it can be used to determine the phase difference, φ, between the acoustic and X-ray signals. Changing the φ value, for example electronically, strongly affects the satellite/main peak ratio, η (see Fig. 4). Since the X-ray temporal structure produced by the APS during these measurements was not completely regular, approximately 25% of the X-ray bursts were not synchronized with the SAW. The non-synchronized bursts contribute to the background level, $\eta_{\rm bg}$, around which the satellite's intensity oscillates (see Fig. 5).

The oscillating dependencies are characterized by double the SAW frequency, 2ν = 1.16 GHz, since the satellite intensity is not sensitive to the sign of the acoustic deformation. In an ideal case, the experimental data should be described by periodic functions: $\eta(t) = \eta_0|\sin[2\pi\nu(t - t_0)]|$, which provide zero satellite's contribution at delay times $t = t_0 + (k/2\nu)$ (k = 0, 1, 2, . . .). However, the finite width of X-ray pulses causes the smearing of the cusps at these points. By adding the background mentioned, the experimental data can be well fitted to the periodic function

$$\eta(t) = \eta_{\rm bg} + \eta_0 \sin\big[4\pi\nu(t - t_0)\big]. \quad (1)$$

In our experiment we measured $\eta(t)$ as a function of the electronic delay time, t, in two $LiNbO_3$ positions, L and L^*, separated by $\Delta L = L^* - L \simeq 3$ cm. Data for 21 keV X-rays are presented in Fig. 6. The shift of the diffractometer with the SAW device on it along the incident X-ray beam leads to an additional time delay, Δt, which is clearly visible when comparing the $\eta(t)$-dependences measured in positions L and L^* (see Fig. 6). Note that to observe the separation between the $\eta(t)$ curves, the ΔL magnitude should be a considerable part of ΔL_0 = 25.85 cm. The Δt value is extracted as a result of fitting the experimental data by functions (1). The L and L^* distances are precisely measured by the laser-scan micrometer. After that, the speed of X-rays is determined by the simple formula

$$c_x = (L^* - L)/\Delta t. \quad (2)$$

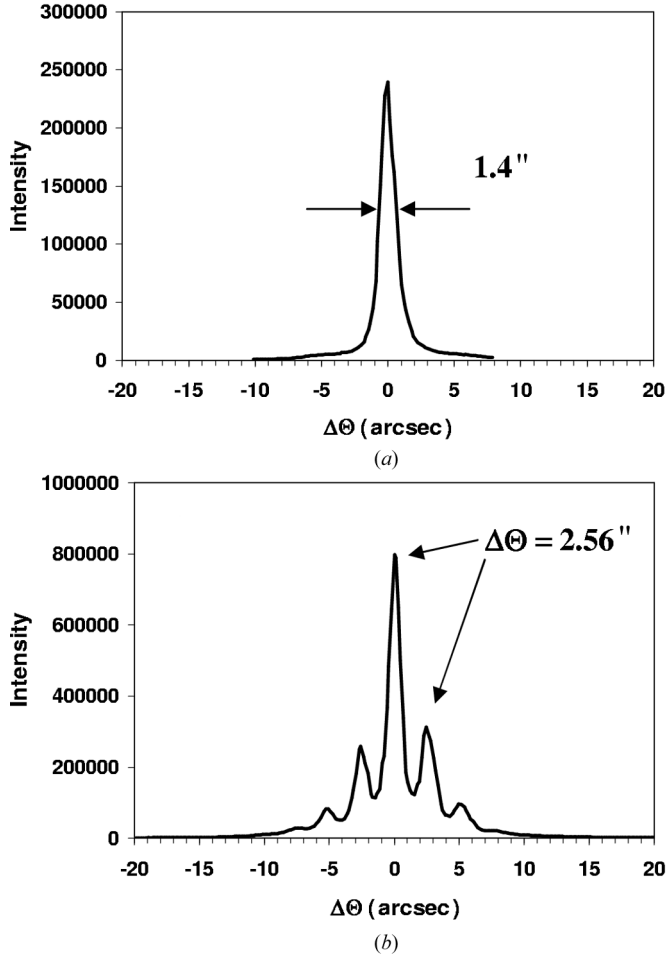

Figure 3
The (060) $LiNbO_3$ rocking curves taken with 21 keV X-rays: (*a*) with no SAW; (*b*) showing pronounced satellite structure under 0.58 GHz SAW excitation.

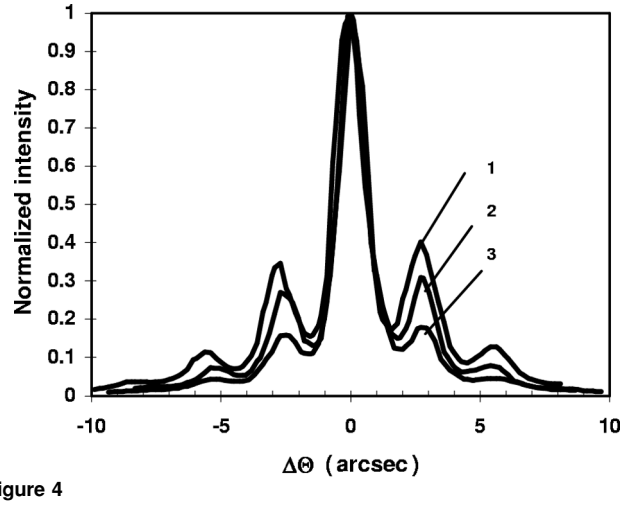

Figure 4
The (060) $LiNbO_3$ rocking curves taken with 21 keV X-rays at three different delay times: 1: 684 ps; 2: 0 ps; 3: 1062 ps; illustrating the change in the satellite intensity.

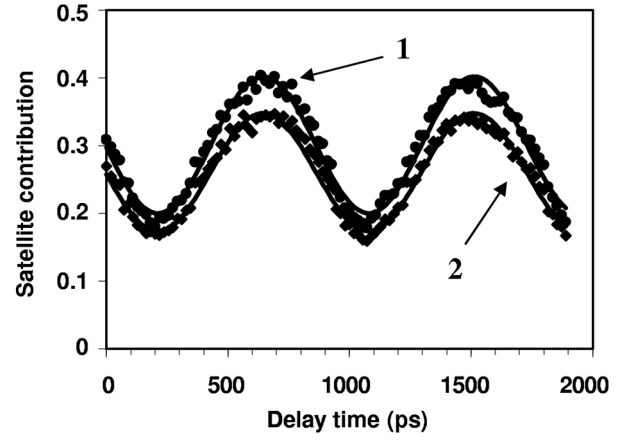

Figure 5
Satellite/main peak ratio [right-side (1) and left-side (2)] for 21 keV X-rays as a function of the delay time at fixed L position. Solid lines represent fittings to equation (1).

The X-ray speed, c_x, as a function of X-ray energy, is plotted in Fig. 7. Averaging over five energy points yields $c_x = (2.983 \pm 0.043) \times 10^8$ m s^{-1}. This is rather close to the tabulated constant, $c = 299792458$ m s^{-1} (see http://www.physics.nist.gov), the relative deviation being $(c_x - c)/c = -5 \times 10^{-3}$.

4. Error analysis

In this section we point out some error sources in order to improve the precision of the future measurements of the speed of X-rays. Main errors are related to time-dependent characteristics of the experimental set-up, including X-ray beams.

4.1. Fluctuations of the diffractometer position

This source of errors may be important because it directly influences the velocity of light according to (2). In order to precisely monitor the diffractometer position, we incorporated the laser micrometre readings into the automated routine for each individual diffraction run. Two typical examples of the tiny diffractometer movements 'at rest' are shown in Fig. 8. First, in Fig. 8(*a*), laser readings were taken every 100 s before any diffractometer move (*i.e.* at position L). The entire monitoring time was almost 4 h. It is seen that even at rest the positional fluctuations are within 400 nm. The second plot (Fig. 8*b*) reflects the dynamics of the diffractometer position after moving for 3 cm and stopping in position L^*. The laser readings were again taken every 100 s, and the entire measurement time was almost 5 h. In the case of diffractometer translation, the 150 kg diffractometer continues to move even after the translation table is stopped and fixed. The diffractometer moved about 2 µm during 2 h, and then was stable. After 2 h, only positional fluctuations within 200 nm were recorded. Recalculating the fluctuation values to the time domain yields jitter of about 1 fs. Thus, the steady-state fluctuations are negligible. Micrometre-scale movements, δL, before complete stop which, in principle, can introduce an error $\Delta c_x/c_x = \delta L/\Delta L \simeq 10^{-4}$ were eliminated by incorporating the laser micrometre readings into the measurement routine.

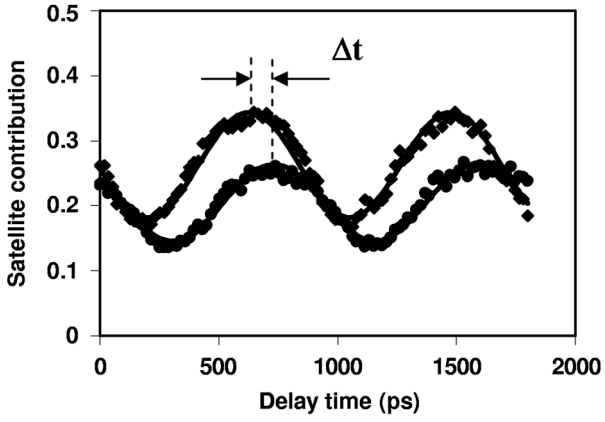

Figure 6
Left-side satellite/main peak ratios measured with 21 keV X-rays at L and L^* positions, as a function of the delay time. Solid lines represent fittings to equation (1). The shift Δt is the additional delay introduced by translating the diffractometer.

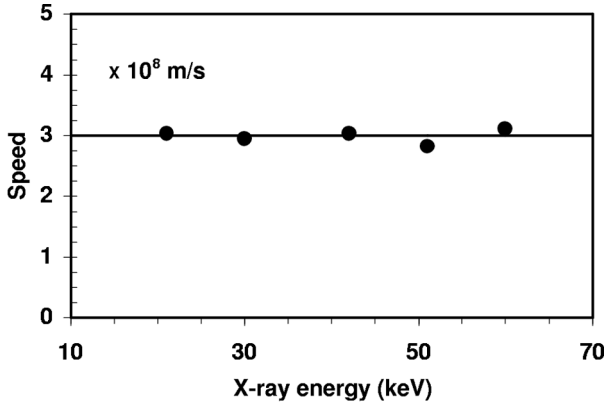

Figure 7
The speed of X-rays, c_x (in 10^8 m s^{-1}), as a function of the X-ray energy. The solid line represents the tabulated value for the speed of light in a vacuum.

4.2. Finite width of X-ray bursts

The width of X-ray bursts at the APS ($\sim$50 ps) is comparable with time intervals, $\Delta t \simeq 100$ ps, introduced by the diffractometer translation of $\Delta L \simeq 3$ cm. Fortunately, for the sine-type modulation of X-ray diffraction intensity which we used in the experiment, this is not so important. In fact, the convolution of the sine function (1) with the Gaussian function, which represents the shape of X-ray bursts, results again in a sine function,

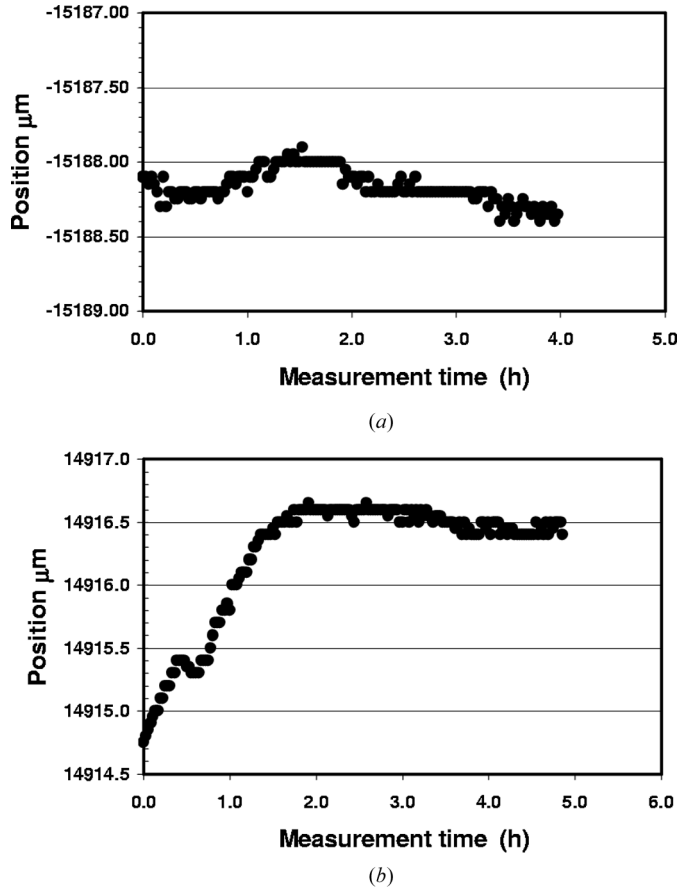

Figure 8
Time-dependent readings (in micrometres) of the laser-scan micrometer during the measurements at 60 keV: (*a*) in the L position; (*b*) in the L^* position.

$$\eta(t) = \eta_{bg} + \frac{\eta_0}{(2\pi)^{1/2}\sigma}\int_{-\infty}^{\infty} \exp\left[-(t-t')^2/2\sigma^2\right]\sin\left[4\pi(t'-t_0)\right]\mathrm{d}t'$$
$$= \eta_{bg} + \eta_0 \exp\left[-8(\pi\sigma\nu)^2\right]\sin\left[4\pi(t-t_0)\right]. \quad (3)$$

The only difference is the reduced oscillation contrast by factor $f = \exp[-8(\pi\sigma\nu)^2]$. As far as $f << 1$, the X-ray burst width may be out of consideration. Conversion to the modulation frequencies yields $\nu << 5$ GHz, which works well in our case of $\nu = 0.58$ GHz.

4.3. Jitter of the electronic delay line

Introducing some averaged error, τ, of time intervals, which represents jitter of the delay line, into (1) and differentiating over t, yields

$$\Delta\eta/\eta_0 = (4\pi\nu\tau)\cos\left[4\pi\nu(t-t_0)\right] \leq (4\pi\nu\tau). \quad (4)$$

Substituting the reasonable value τ = 1–2 ps leads to the rough estimation $\Delta\eta/\eta_0 \simeq 1\%$, which definitely results in the deterioration of the measurement precision, and should be taken into account when analyzing experimental results.

4.4. X-ray intensity variation

Time-dependent intensity variations of the incident X-rays are mainly due to the decay of the electron current in the storage ring and to the electron current refills which are performed periodically. In order to take into account these effects, the diffraction intensity is usually normalized to the monitor signal, which is measured before the sample and is proportional to the incident beam intensity. As a rule, the diffraction intensity follows the in-time variations of the monitor intensity. However, when working with highly restricted incident beams at the sample position, which are much smaller than the 1 × 2 mm beam that passes through the monitoring ionization chamber, the time dependencies of the monitor and the diffraction signals can be different.

Consequently, we normalized the satellite intensity to the main peak intensity, but not to the monitor readings. This allowed us to substantially increase the quality of the $\eta(t)$ data, which are now influenced only by the intensity fluctuations caused by the delay line jitter and measurement statistics. The latter is limited by the narrow slits (required to observe diffraction satellites) and by restricted beam time availability. In turn, the intensity fluctuations limited the accuracy of the phase determination, $\varphi = 4\pi\nu t_0$ [see equation (1)], which is obtained by means of the fitting procedure. Owing to the statistical scattering of the experimental points (see Figs. 5 and 6), the non-linear least-square fits of individual $\eta(t)$ curves provided the t_0 values with standard deviations of about 0.5–2%. Since the speed of X-rays is determined *via* the difference, Δt, of two t_0 values [see equation (2)], the relative errors of the individual speed values increase up to approximately 1–5%. Measurements at higher energies, which are characterized by lower X-ray intensities, reveal more scattering in c_x values (see Fig. 7). Finally, the mean value, c_x, was taken over five energy measurements, which yields the relative standard deviation of the mean value $\delta/c_x = 1.4\%$.

5. Conclusions

Fast stroboscopic X-ray diffraction measurements were performed in order to directly measure the speed of X-rays at different X-ray energies. We accomplished the time-of-flight experiments by using the intrinsic pulsed structure of synchrotron radiation produced by the APS. A 0.58 GHz SAW device served as a temporal analyzer of X-ray arrivals from the storage ring to the device position. Temporal analysis was based on searching the intensity of SAW-induced satellites in diffraction profiles. By changing the delay time between the periodic acoustic deformation and X-ray illumination, we were able to enhance or diminish the satellite intensity. For each X-ray energy, these oscillating dependencies were measured twice, *viz*. for two diffractometer positions separated by a well known spacing. The speed of X-rays, then, was determined as a ratio between measured translation distances and time intervals.

Consequently, for photons up to 60 keV the speed of X-rays, c_x, within the experimental error bars equals the tabulated value of the speed of light in a vacuum, c. The proximity is $(c - c_x)/c = -5 \times 10^{-3}$. The c_x value is averaged over five measurements at different energies, and the relative standard deviation of the mean value is $\delta/c_x = 1.4\%$. Analysis of the possible error sources showed that the measurement precision is mostly influenced by two factors: counting statistics and jitter of electronic delay line. Improving both factors (*e.g.* performing experiments at an insertion-device beamline instead of a bending-magnet beamline) will result in better accuracy, and a level of 10^{-4} is probably achievable.

This work was performed at the DuPont-Northwestern-Dow Collaborative Access Team (DND-CAT) Synchrotron Research Center located at Sector 5 of the APS. DND-CAT is supported by the E. I. DuPont de Nemours & Co., The Dow Chemical Company, the US National Science Foundation through grant DMR-9304725 and the State of Illinois through the Department of Commerce and the Board of Higher Education grant IBHE HECA NWU 96. Use of the APS was supported by the US Department of Energy, Basic Energy Sciences, Office of Energy Research under contract No. W-31-102-Eng-38.

References

Bates, H. E. (1988). *Am. J. Phys.* **56**, 682–687.
Bergstrand, E. (1956). In *Encyclopedia of Physics*, Vol. XXIV, *Fundamentals of Optics*, edited by S. Flugge. Berlin: Springer-Verlag.
Cohen, E. R. & Taylor, B. N. (1987). *Rev. Mod. Phys.* **59**, 1121–1148.
Entin, I. R. & Assur, K. (1981). *Acta Cryst.* A**37**, 769–774.
Froome, K. D. & Essen, L. (1969). *The Velocity of Light and Radio Waves.* London/New York: Academic Press.
Masociovecchio, C., Bergmann, U., Kirsch, M., Ruocco, G., Sette, F. & Verbeni, R. (1996). *Nucl. Instrum. Methods Phys. Res. B*, **111**, 181–186.
Matthews, H. (1977). *Surface Acoustic Wave Filters*. New York: John Willey.
Sanders, J. N. (1965). *Velocity of Light.* Oxford: Pergamon Press.
Sauer, W., Streibl, M., Metzger, T. H., Haubrich, A. G. C., Manus, S., Wixforth, A. & Peisl, J. (1999). *Appl. Phys. Lett.* **75**, 1709–1711.
Taylor, B. N., Parker, W. N. & Langenberg, D. N. (1969). *Rev. Mod. Phys.* **41**, 375–496.
Tucoulou, R., Pascal, R., Brunel, M., Mathon, O., Roshchupkin, D. V., Schelokov, I. A., Cattan, E. & Remiens, D. (2000). *J. Appl. Cryst.* **33**, 1019–1022.
Zolotoyabko, E., Panov, V. & Schvarkov, D. (1993). *Rev. Sci. Instrum.* **64**, 1274–1279.
Zolotoyabko, E. & Polikarpov, I. (1998). *J. Appl. Cryst.* **31**, 60–66.
Zolotoyabko, E., Shilo, D., Sauer, W., Pernot, E. & Baruchel, J. (1998). *Appl. Phys. Lett.* **73**, 2278–2280.
Zolotoyabko, E., Shilo, D., Sauer, W., Pernot, E. & Baruchel, J. (1999). *Rev. Sci. Instrum.* **70**, 3341–3345.